Published in final edited form as:

*ASAIO J.* 2017 ; 63(5): 631–636. doi:10.1097/MAT.0000000000000542.

# Fiber bundle design for an integrated wearable artificial lung

**Shalv. P. Madhani**[*,†], **Brian. J. Frankowski**[*,†], and **William. J. Federspiel**[*,†,‡,§]

[*]McGowan Institute for Regenerative Medicine, University of Pittsburgh, 3025 East Carson Street, Pittsburgh, PA 15203, USA

[†]Department of Bioengineering, University of Pittsburgh, Pittsburgh, PA

[‡]Department of Chemical and Petroleum Engineering, University of Pittsburgh, Pittsburgh, PA

[§]Department of Critical Care Medicine, University of Pittsburgh Medical Center, Pittsburgh, PA

## Abstract

Mechanical ventilation and ECMO are the only viable treatment options for lung failure patients at the end stage, including ARDS and COPD. These treatments however are associated with high morbidity and mortality due to long wait times for lung transplant. Contemporary clinical literature has shown ambulation improves post-transplant outcomes in lung failure patients. Given this, we are developing the PAAL, a truly wearable artificial lung that allows for ambulation. In this study, we targeted 180 ml/min oxygenation and determined the form factor for a hollow fiber membrane (HFM) bundle for the PAAL.

Based on a previously published mass transfer correlation we modeled oxygenation efficiency as a function of fiber bundle diameter. Three benchmark fiber bundles were fabricated to validate the model through *in-vitro* blood gas exchange at blood flow rates from 1 to 4 L/min according to ASTM standards. We used the model to determine a final design, which was characterized in-vitro through a gas exchange as well as a hemolysis study at 3.5 L/min The percent difference between model predictions and experiment for the benchmark bundles ranged from 3% to 17.5% at the flowrates tested. Using the model, we predicted a 1.75 inch diameter bundle with 0.65 $m^2$ surface area would produce 180 ml/min at 3.5 L/min blood flow rate. The oxygenation efficiency was 278 ml/min/$m^2$ and the Normalized Index of Hemolysis (NIH) was less than 0.05g/100L. Future work involves integrating this bundle into the PAAL for which an experimental prototype is under development in our laboratory.

### Keywords

Artificial lung; Hollow fiber membrane; Oxygenator design

Corresponding Author: William J. Federspiel, Ph.D., McGowan Institute for Regenerative Medicine, University of Pittsburgh, 3025 East Carson Street, Pittsburgh, PA 15203, federspielwj@upmc.edu, Phone: +1-412-383-9499, Fax: +1-412-383-9460.

Conflicts of Interest:
Authors do not have conflicts of interest to disclose

## Introduction

Acute and chronic lung disease are major healthcare problems. The CDC reports that lung disease is the third leading cause of death in the United States.[1] Acute respiratory distress syndrome (ARDS) affects 190,000 patients annually and is associated with a mortality of 64%.[2] Chronic lung disease affects 12.7 million annually and is associated with a mortality of 135,000.[3,4] As lung disease becomes end stage, lung transplant is the only viable treatment.[5] The number of lung transplants has been growing at the rate of 179 transplants annually (3519 in 2010),[6] but the supply of organs is not sufficient to meet the need for lung transplants. The Organ Procurement and Transplant Network (OPTN) database states that approximately 2500 patients are added to the wait list annually. The average time of the wait list in 2013 was 4 months varying from 2.6 months to 9.7 months depending on the level of sickness of a patient, and the wait list mortality is 10–15 deaths per 100 patient-years of waiting.[6]

Current intervention techniques include mechanical ventilation (MV) and extracorporeal membrane oxygenation (ECMO). Prolonged MV injures the patient in the form of barotrauma and volutrauma to the lung, and results in poor post-transplant outcomes.[7,8] Conventional ECMO can be used a bridge to transplant but is cumbersome and expensive in addition to being associated with high morbidity and mortality.[9–11] This morbidity and mortality is only exacerbated through progressive deconditioning as patients are confined in MV and ECMO.[12,13] Recently clinical implementation of the Maquet Cardiohelp, or Quadrox along with centrifugal,[14,15] and novel cannula such as the Avalon Elite® (Maquet Cardiovascular LLC, Wayne, NJ) dual lumen cannula have simplified ambulation on ECMO.[16] Ambulation using such systems improves patient outcomes as this allows patients to walk, eat and exercise during therapy – reducing muscle deconditioning.[9,10,17,18] Yet, the newer generation of ECMO systems remain bulky and cumbersome.

We are developing a highly integrated blood pump and oxygenator as a wearable artificial lung or respiratory assist device. By integrating a hollow fiber membrane (HFM) bundle for gas exchange directly with an efficient centrifugal pump, the Pittsburgh Ambulatory Assist Lung (PAAL) is a truly wearable device that allows for patient ambulation. The PAAL requirements based on other device used clinically and under research development include[19–21] a small form factor, long-term (1–3 month) durability, 180 ml/min oxygenation at 3.5 L/min for providing partial to complete lung support, compatibility with the Avalon Elite® DLC and a normalized index of hemolysis (NIH) under 0.05 g/100L.[31] The small form factor can be achieved by minimizing the size of the HFM bundle, which typically represents the largest component of the pump oxygenator system. In turn, a smaller HFM bundle requires a design with increased gas exchange efficiency. Diffusional boundary layers dictate the gas exchange in HFM bundles, with thicknesses that scale approximately as the square root of fluid velocity past the fiber surfaces.[22] Increasing velocity of fluid flow through the fiber bundle thus increases gas exchange efficiency. In other respiratory assist applications, “active mixing” has been used as a means to increase the fluid velocity past fiber surfaces by using ancillary components like rotating impellers adjacent to the fiber bundle or rotating the fiber bundle itself within a stationary housing.[23–26] In this study, we investigated a simpler, passive means to improve mass transfer efficiency in hollow fiber

bundles by manipulating their form factor to increase the fluid velocity past fiber surfaces. We used a simple 1D model of blood flow and gas exchange in hollow fiber bundles based on a previously published mass transfer correlation[24] to characterize oxygenation efficiency as a function of fiber bundle diameter. Various fiber bundles were fabricated to validate the model and to help determine a fiber bundle form factor (diameter – gas exchange surface area) that would oxygenate blood 180 ml/min at 3.5 L/min. The final design was characterized in-vitro through a gas exchange and hemolysis study.

## Methods

### Oxygen Transfer Model

The PAAL specific HFM geometry was modeled using a previously published[27] mass transfer correlation. The mass balance on $O_2$ in the fiber bundle is:

$$Q\frac{dC_{O_2}}{dz} = \pi R^2 k a_v \Delta P_{O_2}(z) \quad (1)$$

where $Q$ is the flowrate through the bundle, $R$ is the bundle radius, $a_v$ is the surface area to volume ratio, $z$ is the axial coordinate, $\Delta P_{O_2}$ is the oxygen partial pressure difference between the fluid and gas sides, $k$ is the mass transfer coefficient.

The oxygen concentration $C_{O_2}(z)$ blood accounting for the dissolved and bound concentration is given by:

$$C_{O_2} = \alpha_{O_2} P_{O_2} + C_T S_{O_2} \quad (2)$$

where, $P_{O_2}$ is the partial pressure of oxygen, $C_T$ is the hemoglobin binding capacity and $S_{O_2}$ is oxygen saturation. The mass transfer coefficient $k$, for oxygen transfer from the inside of the fiber to the blood is:

$$Sh = 0.54 Re^{0.42} Sc^{1/3} \quad (3)$$

$Sh$ is the Sherwood number defined as $Sh = kd_h/\alpha_{O_2} D_{O_2}$ where $\alpha_{O_2}$ and $D_{O_2}$ are the solubility and diffusivity of oxygen in blood, and $d_h$ the hydraulic diameter which is equivalent to the fiber diameter. $Re$ is the reynold's number and is defined as $Re = \rho V d_h/\mu$ where $\rho$ and $\mu$ are fluid density and viscosity, $V$ is the superficial blood flow velocity, $Sc$ is Schmidt number which is $v_b/D_{O_2}$ where $v_b$ is the kinematic viscosity of blood.

The differential equation in (1) was solved using equation (2) and (3) in Matlab (MathWorks®, Natick, MA) with the built in ODE solver based on the Runga-Kutta method. Oxygenation efficiency (oxygenation normalized to surface area) was calculated for the

three benchmark bundles described in Table 1 (FB-1 to FB-3). Following validation, a final bundle geometry (FB-F) was designed using the model.

## Fiber Bundle Manufacturing

Commercially available Membrana® PMP 90/200 type hollow fiber sheets (44 fibers/inch) (Membrana GmbH, Wuppertal, Germany) were used for manufacturing the four fiber bundles in the described in table 1. Bundles were designed to have blood flow over fibers, with gas flowing through the fiber lumen. Square sheets cut from a spool of fiber were die cut and sealed with an arbor-press. These sheets then fit in a round custom potting fixture. The potting fixture contained a glue reservoir attached to a mold in which fibers are stacked alternatingly at a 14° crossing angle; fibers were oriented perpendicular to the principal direction of blood flow. The mold was spun on its axis at 1400 RPM for 12 hours until the polyurethane potting adhesive (Vertellus Performance Materials Inc., Greensboro, NC) cured. Void fraction of the bundles was 0.5. Pressure drop for fiber bundles was estimated using a modified Blake-Kozeny equation. Custom test fixtures shown in Figure 1 housed bundles during experiments.

## In-Vitro Gas Exchange

Gas exchange testing followed ISO 7199 standards[28] using seven liters of locally collected slaughterhouse blood. Bovine or porcine blood was used interchangeably as hill dissociation curves across experiments overlapped. Blood was passed through a 40 μm filter (Pall Biomedical, Inc., Fajardo, PR), and treated with heparin (10 IU/mL) and gentamycin (0.1 mg/mL). The experimental setup consisted of the single pass loop system shown in Figure 2. The loop contained two custom manufactured compliant 6L blood reservoir connected to a Biomedicus BP 80-X pump (Medtronic, Minneapolis, MN) and the test device. Oxygenated blood was deoxygentated with a Medtronic Affinity NT 2.5$m^2$ oxygenator (Medtronic, Minneapolis, MN) placed downstream of the test device. Blood temperature was maintained at 37C with a PolyScience 210 heater (PolyScience Inc., Niles, IL) connected to the deoxygenates's built in heat exchanger. Standard R-3603 Tygon tubing (Cole-Parmer, Vernon Hills, IL) connected loop components.

Prior to collecting a data point, a blend of $N_2$, $CO_2$, $O_2$ sweep gas were flowed through the deoxygenator, conditioning blood to have an oxygen saturation of 65% ±5% and a $pCO_2$ of 45 mmHg ± 5 mmHg. Once conditioned, blood passed from the inlet reservoir through the loop into the outlet reservoir such that the post device blood was separate from the conditioned blood at all times. Flowrates tested were 1, 2, 3, 3.5 and 4 L/min. An ultrasound flow probe (Transonic Systems Inc., Ithaca, NY) measured flow. Pure oxygen sweep gas flowed through the test device at 7.5 L/min, measured with a GR Series mass flow controller (Fathom Technologies, Georgetown, TX). Each point was repeated once. One sample was drawn from each of the sampling ports shown in Figure 2. A Rapid Point 405 Blood Gas Analyzer with Co-oximetry (Siemens Healthcare Diagnostics Inc., Tarrytown, NY) measured blood gases and oxygen saturation.

Oxygen transfer rates were calculated as:

$$\dot{V}_{O_2} = Q[\alpha_{O_2}(\Delta P_{O_2}) + C_T \Delta S_{O_2}] \quad (4)$$

Where $\dot{V}_{O_2}$ is the rate of oxygenation, $Q$ is the blood flowrate, $\alpha_{O_2}$ is the oxygen solubility in blood $\left(3 \times 10^5 \frac{ml_{O_2}}{ml_{blood}\, mmHg}\right)$, $\Delta P_{O_2}$ is the partial pressure difference across the device, $C_T$ is the binding capacity $(0.167 \frac{ml_{O_2}}{ml_{blood}})$, and $\Delta S_{O_2}$ is the saturation difference across the device.

### In-Vitro Hemolysis

Hemolysis testing followed established standards.[29,30] Testing comprised of two identical loops in which flow was driven using a Centrimag blood pump (Thoratec, Pleasanton, CA) and measured using an ultrasound flow probe. A 1200 mL compliant blood reservoir (Medtronic, Minneapolis, MN) was used for each loop. Temperature was maintained at 37C using a water bath and heat exchanger. The test loop comprised of a fiber bundle module and a 27 Fr. Avalon Elite® DLC (Maquet Cardiovascular LLC, Wayne, NJ) in addition to the Centrimag pump. The control loop comprised of just the cannula and pump.

Both loops ran simultaneously at 3.5 L/min for a shortened duration of 3 hours owing to the linearity in the trend between plasma-free hemoglobin (PfHb) and time ($R^2 > 0.9$). Every half-hour, one 3 mL waste sample was pulled from each loop before drawing one 5 mL sample. PfHb was tracked using this 5ml sample. The supernatant was taken from the sample after centrifuging at 800 g for 15 minutes, and then spun at 7200 g for 10 minutes. The absorbance of the purified plasma was measured at 540 nm using a Genesys 10 UV-vis spectrophotometer (Thermo Fisher Scientific, Waltham, MA). PfHb was calibrated to absorbance by generating linear standard curves (n=3) prior to the experiment. These standard curves correlated PfHb to absorbance via a slope of 0.11 g/dL/A. Hematocrit was measured using a capillary tube in a IEC Mb micro-centrifuge (International Equipment Co., Needham Hts, MA).

Blood damage was then expressed as a normalized index of hemolysis (NIH) which normalizes the rate of change of PfHb $\left(\frac{dPfHb}{dt}\right)$ to loop volume ($V$), hematocrit ($Hct$), and blood flowrate ($Q$) using the following relationship[30]:

$$NIH = \frac{dPfHb}{dt} V \left(\frac{100 - Hct}{100}\right)\left(\frac{100}{Q}\right) \quad (4)$$

## Results

Benchmark HFM bundle model calculations and experiment values are shown in Figure 3. The percent difference between the model calculations and experiment results ranged from

4.9–13.3% for FB-1 shown in 3A, 3% – 17.5% for FB-2 shown in 3B and 10.4% – 14.6% for FB-3 shown in 3C. Oxygenation efficiency increased as fiber bundle diameter was reduced. At 3.5 L/min $PO_2$ (mmHg) across fiber bundle increased from: 48 to 68 for FB-1, 43 to 76 for FB-2, 47 to 78 for FB-3.

The model was then used to predict the FB-F geometry that would achieve our target oxygenation performance of 180 ml/min at 3.5 L/min Manufacturing constraints relating to the centrifugal potting of fiber bundles prevented further reduction of fiber bundle diameter below 1.75 inches. Oxygenation performance of FB-F is shown in Figure 4. Oxygenation increased from 79 ml/min to 207 ml/min as flowrate was increased from 1L/min to 4 L/min. Oxygenation of 180.7 ml/min, oxygenation efficiency of 278 ml/min/$m^2$ and a $PO_2$ (mmHg) change from 40 to 79 was achieved at 3.5 L/min. Figure 5 shows the NIH of FB-F. The test condition had an NIH of 0.021g/100L while the control had an NIH of 0.018 g /100L.

## Discussion

MV and ECMO are the only viable treatment options for lung failure patients at the end stage, including ARDS and COPD. These treatments however are associated with high morbidity and mortality due to long wait times for lung transplant.[9–13] Contemporary clinical literature has shown ambulation improves outcomes in lung failure patients.[9,10,17,18] Given this, we are developing the Pittsburgh Ambulatory Assist Lung or PAAL, a truly wearable, compact artificial lung that allows for patient ambulation during bridge to recovery or transplant. In this study, FB-F met our design target of 180 ml/min oxygenation despite a low (0.65$m^2$) surface area. The FB-F design has a relatively high efficiency of 278 ml/min/$m^2$, almost two times higher than standard blood oxygenators used for ECMO today. [21] FB-F will be incorporated in the final PAAL device for future bench and animal testing.

Our study found that decreasing the fiber bundle diameter and increasing fiber bundle length increases oxygenation efficiency while still maintaining a low level of hemolysis (NIH 0.021g/100L). The overall contribution of the bundle to hemolysis is ~14% of the total measured hemolysis, given that the baseline level of hemolysis is NIH 0.018g/100L. Albeit low, the cannula and loop generate a larger part of the measured hemolysis. Further, these NIH values are within the acceptable limits (NIH < 0.05 g/100L) of hemolysis for clinically approved oxygenators.[31] As blood flows over HFMs, a fluid boundary layer forms at the surface of the fibers. The thickness of the boundary layer is related to flow velocity past fibers.[22] In this study, the flow velocity is increased by maintaining constant blood flow but reducing frontal area of fiber bundles. Though path length is increased, the increased enhancement is due to velocity increase as residence time is slightly reduced with increasing path length (residence time is 2.1s for FB-F, 2.8s for FB-1). Devices in the past have utilized “active mixing” to reduce boundary layer thickness[23–26] however in this study we achieved this through a simple geometric means thus ensuring low hemolysis.

There are other artificial lung devices under research development for treating patients with lung failure.[14,19,20,21,32,33] The ambulatory pump lung (APL) device features a fully magnetically levitated centrifugal pump integrated into a 0.8$m^2$ surface area annular fiber bundle[19] having 200 ml/min/$m^2$ oxygenation efficiency. The compliant thoracic artificial

lung (cTAL) features a pumpless device with a 2.4$m^2$ surface area bundle having ~95 ml/min/$m^2$ oxygenation efficiency. The device is implanted in the patient's thoracic cavity, relying upon the patient's right ventricular function to pump blood through the device.[20] FB-F designed in this study has 40% higher efficiency than the APL and 200% higher efficiency than the cTAL. Higher oxygenation efficiency ultimately translates into lower required fiber bundle surface area, which not only helps create a more compact artificial lung but also potentially reduces the adverse blood – material interactions associated with a larger blood contacting area.

Our design leads to a path length of 3.12 inches across the fiber bundle. This is longer than the APL (0.85 inch) and cTAL (1.49 inch) devices. At each of their respective operating conditions residences times in these devices are: 1.97s in the APL and 6s–9s in the.[19.20] However, the residence time in FB-F is 2.1s at the operating flowrate of 3.5 L/min. This time is within the range of the APL and cTAL devices which have been tested in vivo up to 30 days with few biocompatibility issues. Further the surface area of FB-F is smallest compared to and other device which potentially mitigates biocompatibility issues. Additionally, some oxygenators used clinically such as the Sorin Inspire have long path lengths as well.[34] As part of the PAAL project we are also developing novel thromboresistant coatings[35] for the PAAL fiber bundle. Overall, we do not expect that the long bundle length used in the PAAL will induce significant hemocompatibility issues. One final point is that the circular cross section of our fiber bundle minimizes dead flow zones which can occur in square cross section oxygenators such as the Quadrox, which is currently the oxygenator used in the Maquet Cardiohelp portable ECMO system.

In conclusion, studies based on 3 benchmark fiber bundles validated our gas exchange model and based on this model, we developed a 0.65$m^2$ fiber bundle that met our target of providing 180 ml/min of oxygenation at 3.5 L/min blood flowrate. The overall oxygenation efficiency was high (278 ml/min/$m^2$), while blood hemolysis was low (NIH 0.021 g/100L). Future work involves integrating this fiber bundle design with a centrifugal pump we are developing into a single housing to create a highly integrated, compact and wearable artificial lung. The integration will be guided by CFD analysis to create a first-generation PAAL prototype for bench and animal validation studies.

## Acknowledgments

This study was supported by NIH grant number RO1 HL117637, the Commonwealth of PA and the McGowan Institute for Regenerative Medicine.

Source of Funding:

This work has received funding from the NIH.

## References

1. [Accessed January 12, 2016] FastStats Available at: http://www.cdc.gov/nchs/fastats/leading-causes-of-death.htm
2. Figueira JF, Oliveros MO, López JL, Civantos BC, Fernández LF. Acute respiratory distress syndrome: analysis of incidence and mortality in a university hospital critical care unit. Critical Care. 2012; 16:P396.

3. Mannino DM. Copd*: Epidemiology, prevalence, morbidity and mortality, and disease heterogeneity. Chest. 2002; 121:121S–126S. [PubMed: 12010839]
4. Chronic Obstructive Pulmonary Disease (COPD) Fact Sheet. [Accessed August 9, 2015] American Lung Association Available at: http://www.lung.org/lung-disease/copd/resources/facts-figures/COPD-Fact-Sheet.html
5. Kotloff RM, Thabut G. Lung Transplantation. Am J Respir Crit Care Med. 2011; 184:159–171. [PubMed: 21471083]
6. Christie JD, Edwards LB, Kucheryavaya AY, et al. The Registry of the International Society for Heart and Lung Transplantation: 29th Adult Lung and Heart-Lung Transplant Report—2012. The Journal of Heart and Lung Transplantation. 2012; 31:1073–1086. [PubMed: 22975097]
7. Villar J, Blanco J, Añón JM, et al. The ALIEN study: incidence and outcome of acute respiratory distress syndrome in the era of lung protective ventilation. Intensive Care Med. 2011; 37:1932–1941. [PubMed: 21997128]
8. Nieman GF, Gatto LA, Bates JHT, Habashi NM. Mechanical ventilation as a therapeutic tool to reduce ards incidence. Chest. 2015
9. MacLaren G, Combes A, Bartlett RH. Contemporary extracorporeal membrane oxygenation for adult respiratory failure: life support in the new era. Intensive Care Med. 2011; 38:210–220. [PubMed: 22147116]
10. Garcia JP, Iacono A, Kon ZN, Griffith BP. Ambulatory extracorporeal membrane oxygenation: a new approach for bridge-to-lung transplantation. J Thorac Cardiovasc Surg. 2010; 139:e137–139. [PubMed: 20219215]
11. Strueber M. Artificial Lungs: Are We There yet? Thoracic Surgery Clinics. 2015; 25:107–113. [PubMed: 25430434]
12. Biscotti M, Sonett J, Bacchetta M. ECMO as Bridge to Lung Transplant. Thoracic Surgery Clinics. 2015; 25:17–25. [PubMed: 25430426]
13. Maury G, Langer D, Verleden G, et al. Skeletal Muscle Force and Functional Exercise Tolerance Before and After Lung Transplantation: A Cohort Study. American Journal of Transplantation. 2008; 8:1275–1281. [PubMed: 18444941]
14. Haneya A, Philipp A, Foltan M, et al. First experience with the new portable extracorporeal membrane oxygenation system Cardiohelp for severe respiratory failure in adults. Perfusion. 2012; 27:150–155. [PubMed: 22249962]
15. Palanzo D, Qiu F, Baer L, Clark JB, Myers JL, Ündar A. Evolution of the Extracorporeal Life Support Circuitry. Artificial Organs. 2010; 34:869–873. [PubMed: 21092028]
16. Wang D, Zhou X, Liu X, Sidor B, Lynch J, Zwischenberger JB. Wang-Zwische Double Lumen Cannula—Toward a Percutaneous and Ambulatory Paracorporeal Artificial Lung. ASAIO Journal. 2008; 54:606–611. [PubMed: 19033774]
17. Perme CS, Southard RE, Joyce DL, Noon GP, Loebe M. Early Mobilization of LVAD Recipients Who Require Prolonged Mechanical Ventilation. Tex Heart Inst J. 2006; 33:130–133. [PubMed: 16878612]
18. Pruijsten R, van Thiel R, Hool S, Saeijs M, Verbiest M, Miranda DR. Mobilization of patients on venovenous extracorporeal membrane oxygenation support using an ECMO helmet. Intensive Care Med. 2014; 40:1595–1597. [PubMed: 25112500]
19. Zhang J, Taskin ME, Koert A, et al. Computational Design and In Vitro Characterization of an Integrated Maglev Pump-Oxygenator. Artificial Organs. 2009; 33:805–817. [PubMed: 19681842]
20. Schewe RE, Khanafer KM, Arab A, Mitchell JA, Skoog DJ, Cook KE. Design and In Vitro Assessment of an Improved, Low-Resistance, Compliant Thoracic Artificial Lung. ASAIO J. 2012; 58:583–589. [PubMed: 23103694]
21. Maquet Cardiohelp Technical Data Sheet:
22. Federspiel WJ, , Henchir KA. Encyclopedia of Biomaterials and Biomedical Engineering Taylor & Francis: 2013 Lung, Artificial: Basic Principles and Current Applications; 910921
23. Jeffries RG, Frankowski BJ, Burgreen GW, Federspiel WJ. Effect of Impeller Design and Spacing on Gas Exchange in a Percutaneous Respiratory Assist Catheter. Artificial Organs. 2004; 38:1007–1017.

24. Svitek RG, Frankowski BJ, Federspiel WJ. Evaluation of a Pumping Assist Lung That Uses a Rotating Fiber Bundle. ASAIO J. 2005; 51:773–780. [PubMed: 16340367]
25. Wu ZJ, Gartner M, Litwak KN, Griffith BP. Progress toward an ambulatory pump-lung. The Journal of Thoracic and Cardiovascular Surgery. 2005; 130:973–978. [PubMed: 16214507]
26. Makarewicz AJ, Mockros LF, Anderson RW. A Pumping Intravascular Artificial Lung with Active Mixing. Journal. 1993; 39
27. Svitek RG, Federspiel WJ. A Mathematical Model to Predict CO2 Removal in Hollow Fiber Membrane Oxygenators. Ann Biomed Eng. 2008; 36:992–1003. [PubMed: 18347984]
28. ISO 7199:2009 Cardiovascular implants and artificial organs -- Blood-gas exchangers (oxygenators). 2009
29. ASTM F1841-97 Standard Practice for Assessment of Hemolysis in Continuous Flow Blood Pumps. 2013
30. Koller T, Hawrylenko A. Contribution to the in vitro testing of pumps for extracorporeal circulation. J Thorac Cardiovasc Surg. 1967; 54:22–29. [PubMed: 6027856]
31. Kawahito, Shinji, et al. Blood trauma induced by clinically accepted oxygenators. ASAIO journal. 2001; 47(5):492–495. [PubMed: 11575824]
32. Leverett LB, Hellums JD, Alfrey CP, Lynch EC. Red Blood Cell Damage by Shear Stress. Biophys J. 1972; 12:257–273. [PubMed: 5016112]
33. De Bartolo C, Nigro A, Fragomeni G, et al. Numerical and Experimental Flow Analysis of the Wang-Zwische Double-Lumen Cannula. ASAIO Journal. 2011; 57:318–327. [PubMed: 21654494]
34. [Accessed June 29, 2016] Sorin Group Products, Inspire Product Line Available at: http://www.sorin.com/products/cardiac-surgery/perfusion/oxygenators/inspire
35. Ye S-H, Arazawa DT, Zhu Y, et al. Hollow Fiber Membrane Modification with Functional Zwitterionic Macromolecules for Improved Thromboresistance in Artificial Lungs. Langmuir. 2015; 31:2463–2471. [PubMed: 25669307]

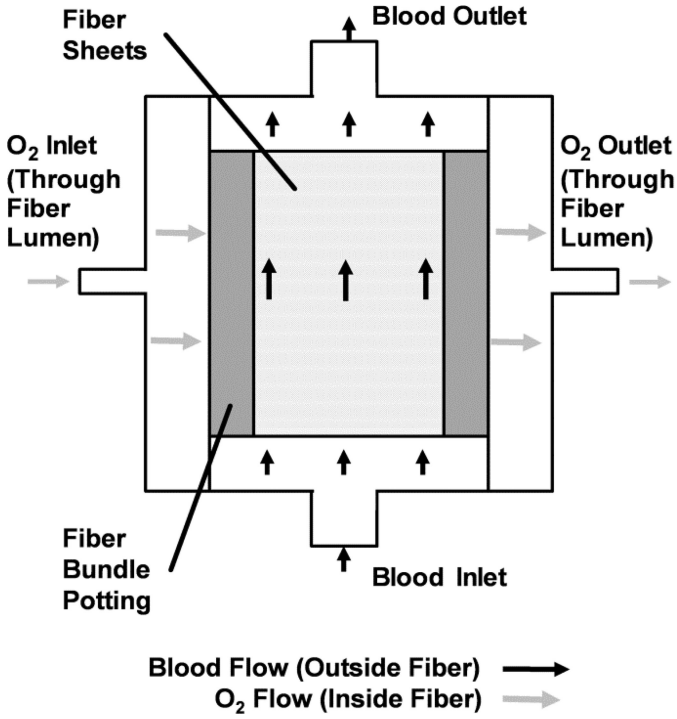


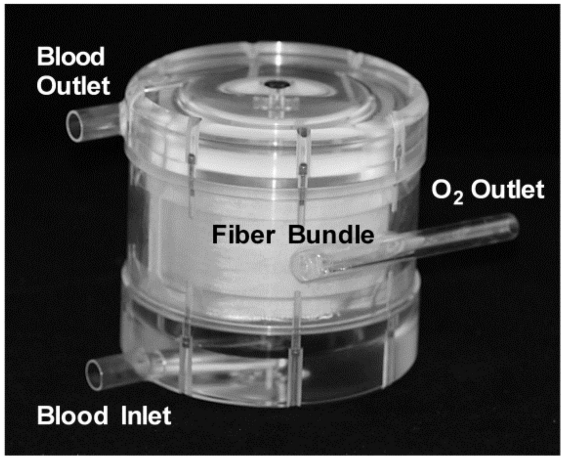


**Figure 1.**

Schematic and prototype of an assembled test module. The schematic indicates components and flow paths through the test module. The bundle is assembled into a custom machined test housing shown in the image of the prototype.

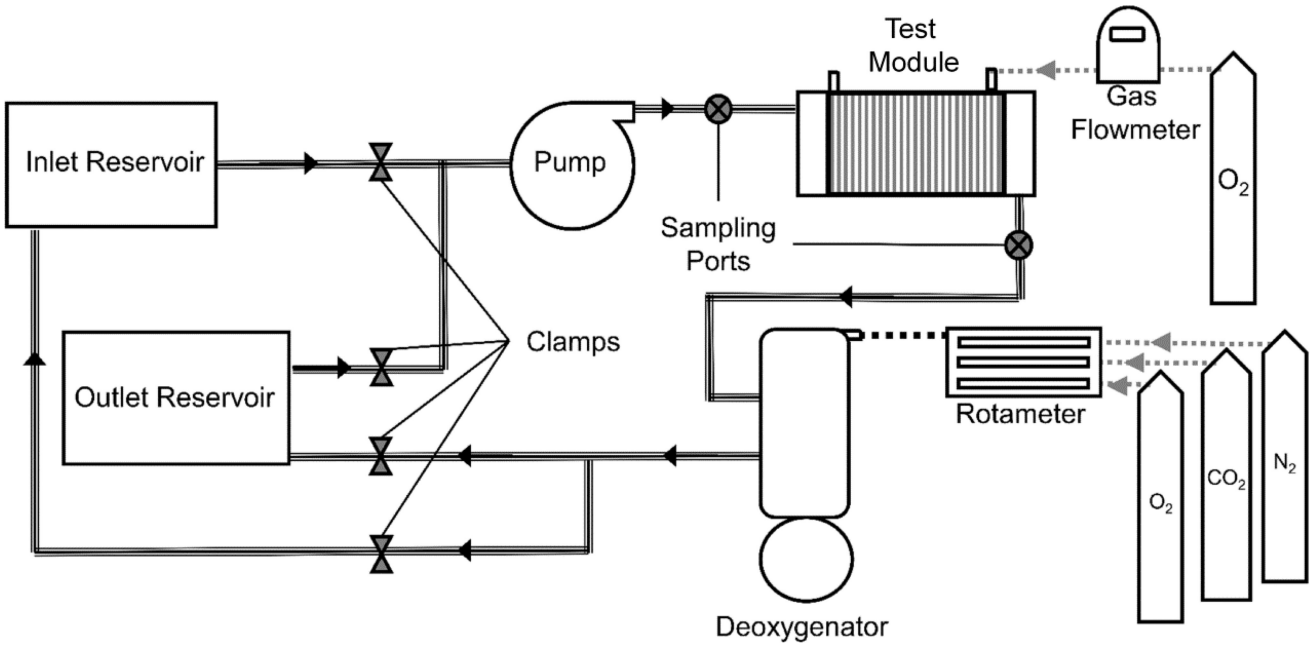


**Figure 2.**

The single pass loop system for measuring in-vitro gas exchange in blood. Clamps at the inlet and outlet reservoir are used to control blood flow through the circuit. Once conditioned, blood passed from the inlet reservoir through the loop into the outlet reservoir keeping the post device blood was separate from the conditioned blood.

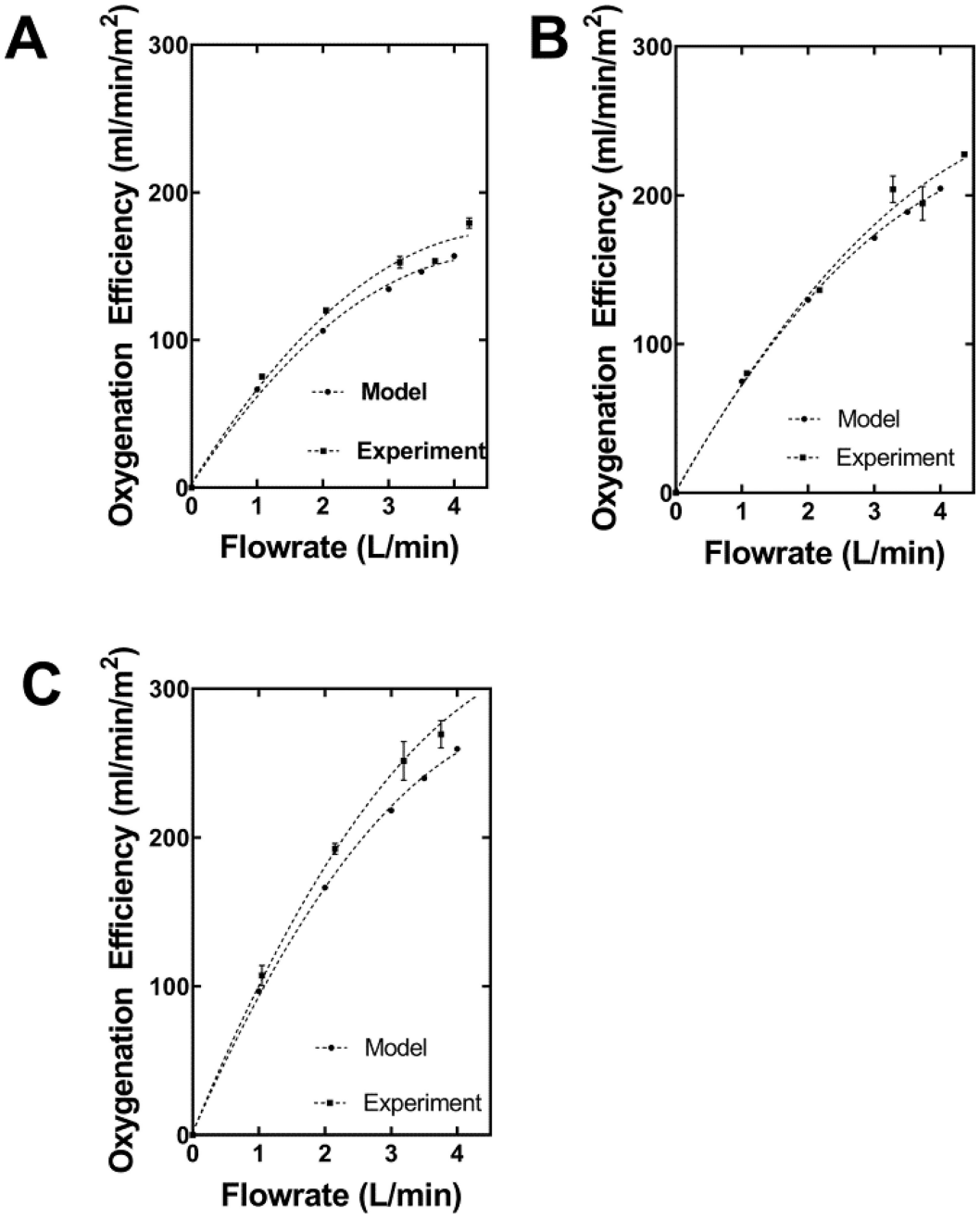


**Figure 3.**

Model calculations and experimental results of oxygenation efficiency (oxygenation per unit surface area) versus flowrate for the FB-1 (Figure 3A), FB-2 (Figure 3B), and FB-3 (Figure 3C).

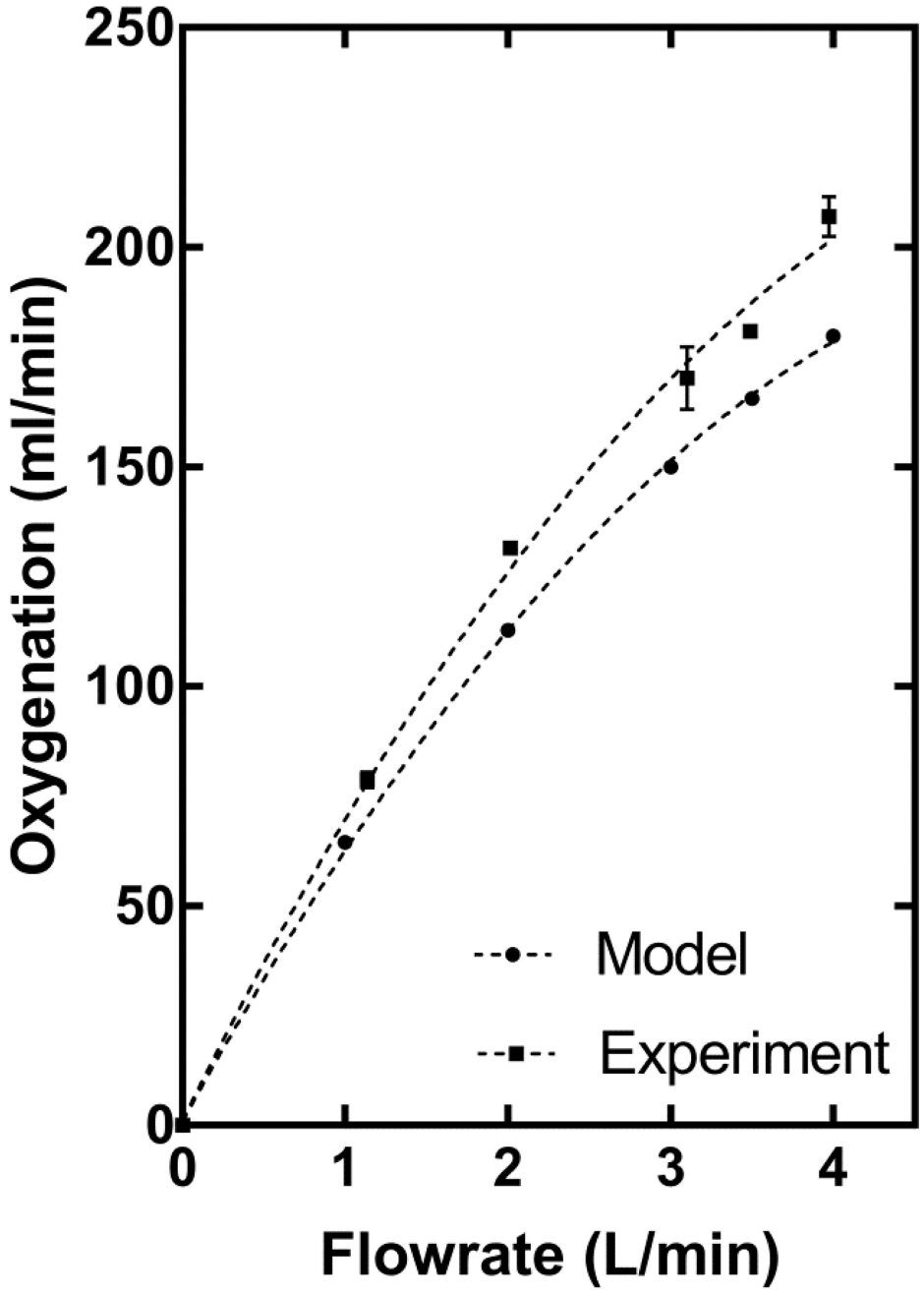


**Figure 4.**

Oxygenation performance of the FB-F fiber bundle determined using the validated gas exchange model. Model predictions are also shown for reference. The bundle meets the oxygenation target (180 ml/min) at 3.5 L/min.

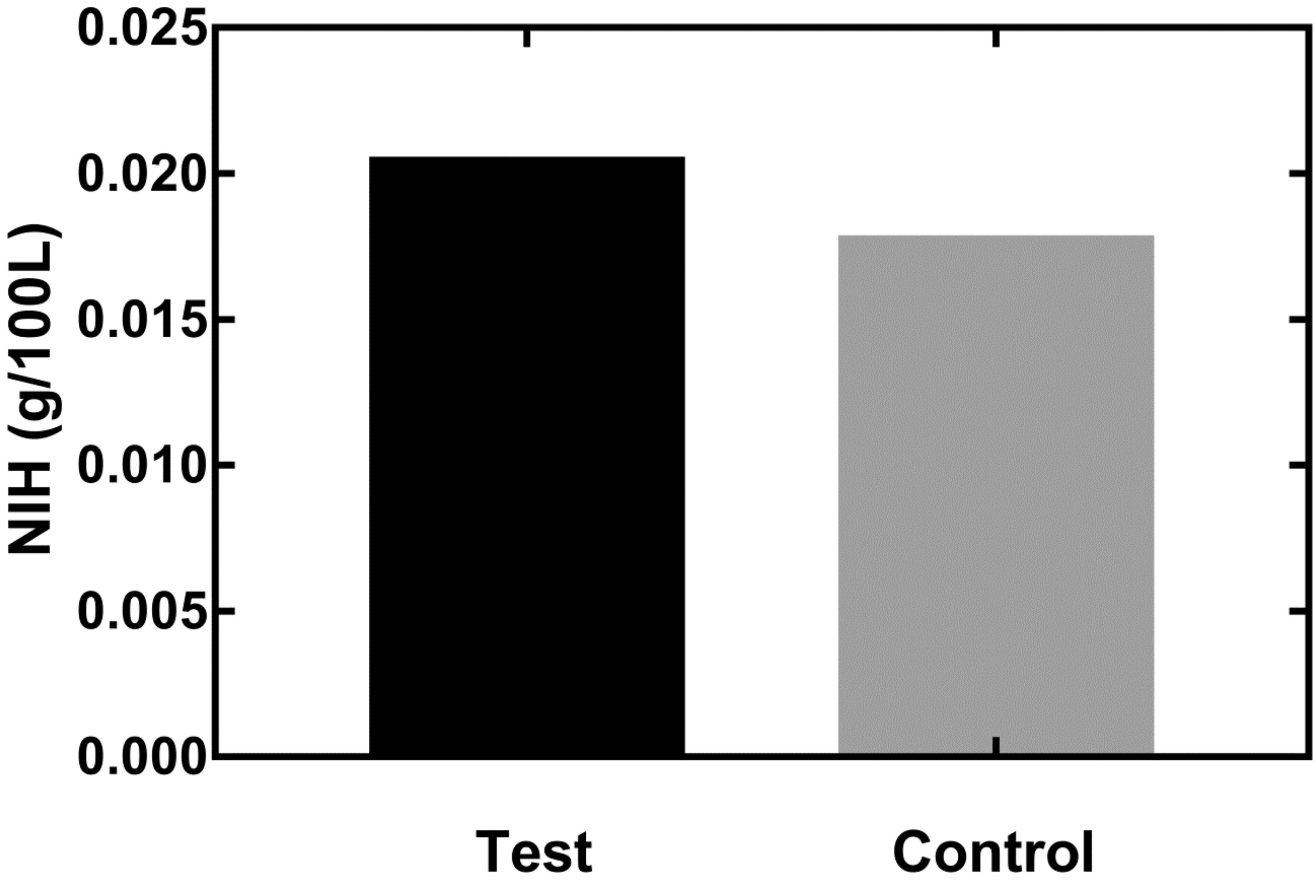


**Figure 5.**

Normalized index of hemolysis (NIH) of the full system and control loops. Both tests were run for 3h at a blood flow of 3.5 L/min. PfHb was measured once every 30 minutes.

**Table 1**

Bundle form factors manufactured for in-vitro testing

| Bundle Name | Bundle Diameter (inch) | Bundle Surface Area ($m^2$) | Number of Sheets | Bundle Length (inch) | Calculated Pressure Drop (mmHg) |
|---|---|---|---|---|---|
| FB-1 | 3.85 | 0.85 | 56 | 0.88 | 4.0 |
| FB-2 | 2.55 | 0.85 | 125 | 2.00 | 20.6 |
| FB-3 | 1.95 | 0.65 | 165 | 2.59 | 45.7 |
| FB-F | 1.75 | 0.65 | 200 | 3.12 | 70.1 |